ADVANCED MATERIALS
www.advmat.de

Systemic Multifunctional Nanovaccines for Potent Personalized Immunotherapy of Acute Myeloid Leukemia

Peng Zhang, Tanzhen Wang, Guanhong Cui, Ruonan Ye, Wenjun Wan, Tianhui Liu, Yiran Zheng,* and Zhiyuan Zhong**

Hematological malignancies (HM) like acute myeloid leukemia (AML) are often intractable. Cancer vaccines possibly inducing robust and broad anti-tumor immune responses may be a promising treatment option for HM. Few effective vaccines against blood cancers are, however, developed to date partly owing to insufficient stimulation of dendritic cells (DCs) in the body and lacking appropriate tumor antigens (Ags). Here it is found that systemic multifunctional nanovaccines consisting of nucleotide-binding oligomerization domain-containing protein 2 (NOD2) and Toll-like receptor 9 (TLR9) agonists – muramyl dipeptide (MDP) and CpG, and tumor cell lysate (TCL) as Ags (MCA-NV) induce potent and broad immunity against AML. MCA-NV show complementary stimulation of DCs and prime homing to lymphoid organs following systemic administration. Of note, in orthotopic AML mouse models, intravenous infusion of different vaccine formulations elicits substantially higher anti-AML efficacies than subcutaneous administration. Systemic MCA-NV cure 78% of AML mice and elicit long-term immune memory with 100% protection from rechallenging AML cells. Systemic MCA-NV can also serve as prophylactic vaccines against the same AML. These systemic nanovaccines utilizing patient TCL as Ags and dual adjuvants to elicit strong, durable, and broad immune responses can provide a personalized immunotherapeutic strategy against AML and other HM.

1. Introduction

Therapeutic vaccines have demonstrated promising potential in curing solid tumors.[1] Cancer vaccines are designed to promote antigen-presenting cells (APCs) such as dendritic cells (DCs) to present loaded tumor antigens (Ags) to T cells, thus inducing T cell immunity to specifically eradicate Ag-expressing tumor cells.[2] With an appropriate repertoire of Ags and adjuvants, cancer vaccines can elicit robust and broad immune responses for tumor eradication. Nevertheless, cancer vaccines have only yielded marginal survival benefits in blood cancer patients so far.[3]

One main contributing factor is that insufficient immune responses were generated by these subcutaneously-applied cancer vaccines. Hematological malignancies (HM) are usually systemic and aggressive with large quantities of cancer cells disseminated in bone marrow, lymph nodes (LNs), spleen, peripheral blood, or other organs.[4] However, subcutaneous vaccines rely on tumor-specific T cells generated at injection sites or in draining LNs to migrate to disease sites for tumor cell killing, thus failing to treat HM efficiently and promptly. It has been reported that systemic application of cancer vaccines could allow delivery of vaccine content to DCs in body-wide lymphoid compartments such as LNs, spleen, and bone marrow.[5] As the location of anti-tumor immunity generated by systemic vaccines mostly overlaps with where AML cells accumulate,[5] we hypothesized that systemic vaccines might elicit more direct and robust killing of blood cancer cells.

Recently, intravenously infused cancer vaccines demonstrated substantially improved therapeutic efficacies than the same vaccines administered subcutaneously in certain murine solid tumor models and yielded encouraging results in patients.[1a,6] However, systemic vaccines for blood cancers are yet to be explored. Acute myeloid leukemia (AML) is the most difficult-to-treat HM and effective anti-AML therapy is lacking, resulting in the low 5-year survival rate (<50%) for AML patients.[4,7] Therefore, developing potent intravenously-infused vaccines against AML might serve as a proof of concept that systemic cancer vaccine is a more effective treatment option for blood cancers.

Tumor cell lysate (TCL) is a promising source of tumor Ags as TCL generated from leukemia cells contains abundant

P. Zhang, G. Cui, R. Ye, Z. Zhong
Biomedical Polymers Laboratory
College of Chemistry
Chemical Engineering and Materials Science, and State Key Laboratory of Radiation Medicine and Protection
Soochow University
Suzhou 215123, P. R. China
E-mail: zyzhong@suda.edu.cn

T. Wang, T. Liu
National Clinical Research Center for Hematologic Diseases
Jiangsu Institute of Hematology
The First Affiliated Hospital of Soochow University
Collaborative Innovation Center of Hematology
Soochow University
Suzhou 215000, P. R. China
E-mail: liutianhui@suda.edu.cn

W. Wan, Y. Zheng, Z. Zhong
College of Pharmaceutical Sciences
Suzhou International Joint Laboratory for Diagnosis and Treatment of Brain Diseases
Soochow University
Suzhou 215123, P. R. China
E-mail: yrzheng@suda.edu.cn

The ORCID identification number(s) for the author(s) of this article can be found under https://doi.org/10.1002/adma.202407189

DOI: 10.1002/adma.202407189

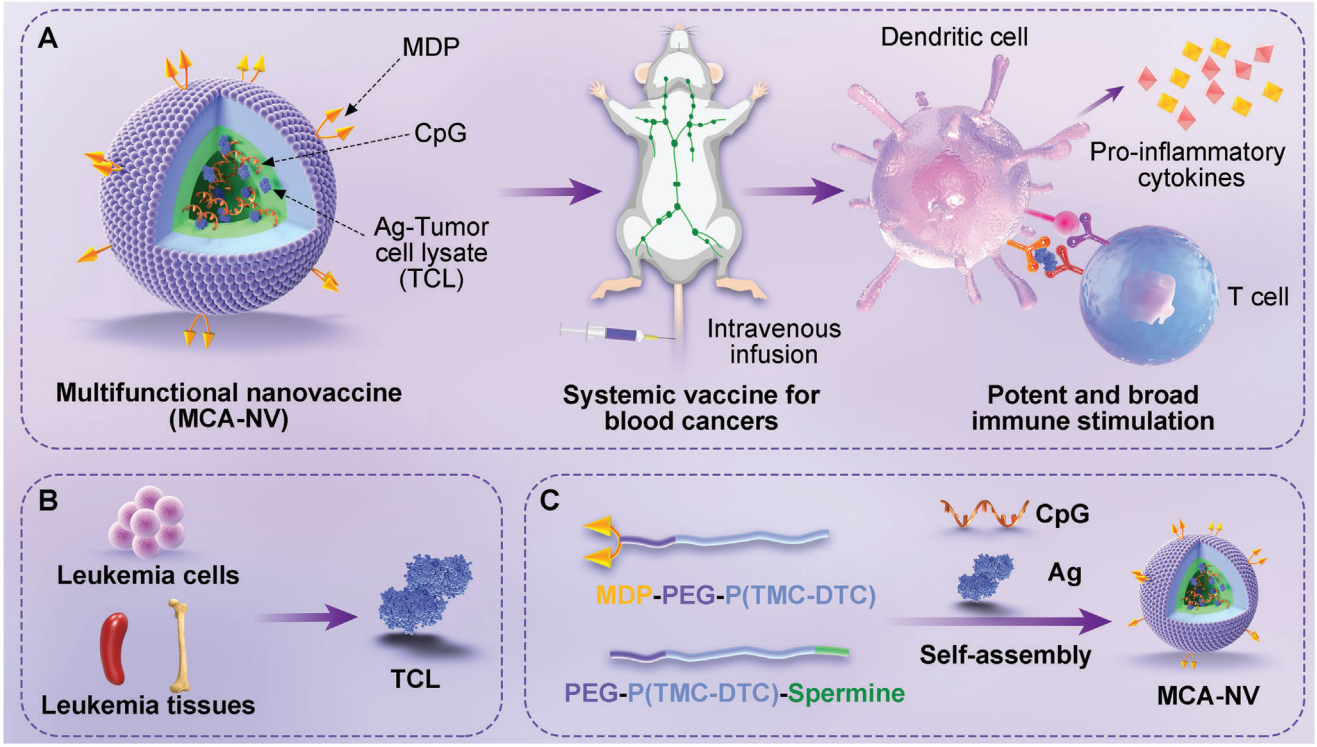

Scheme 1. A) Intravenously-infused multifunctional nanovaccines MCA-NV stimulate robust and systemic immune responses against hematological malignancies. B) Generation of tumor cell lysate (TCL) for vaccine antigens (Ags). C) Preparation of nanovaccines co-loading dual adjuvants – CpG and MDP as well as Ags TCL (MCA-NV) via self-assembly.

and diverse tumor-associated antigens (TAAs) and personalized neoantigens.[8] Thus, TCL-based cancer vaccines can induce broad and personalized anti-AML immune responses to address heterogeneity, a notorious trait of AML, and reduce relapse caused by residual cancer cells.[8a,c] Furthermore, employing TCL as Ags does not require prior knowledge of Ag identity and a suitable number of leukemia cells can be readily harvested from blood or bone marrow.[9]

Immunostimulatory adjuvants are also paramount to effective cancer vaccines.[2a,10] Toll-like receptors (TLRs) and nucleotide-binding oligomerization domain (NOD)-like receptors (NLRs) are among the five main classes of pattern recognition receptors (PRRs) in innate immunity.[11] CpG oligodeoxynucleotides (CpG-ODN), a potent TLR9 agonist, can activate DCs, macrophages, and B cells to drive a strong Th1 inflammatory response.[12] CpG has been approved as an adjuvant in hepatitis B virus vaccine and has demonstrated encouraging potential in cancer vaccine studies.[2a,13] Muramyl dipeptide (MDP), a minimal and conserved peptidoglycan of bacteria cell walls, is an effective agonist to nucleotide-binding oligomerization domain-containing protein 2 (NOD2), a type of NLRs.[14] MDP can potently induce immune activation through NF-κB and AP-1 signaling and has entered cancer vaccine clinical trials.[15] The interplay between different classes of PRRs allows coordinated and enhanced pathogen sensing and immune activation.[16] Combining CpG and MDP can engage both TLR9 and NOD2 to activate different pathogen sensing mechanisms, thus amplifying the NF-κB, AP-1, and IRF signals for more potent immune activation.[2a,15b,17] Furthermore, TLR9 is expressed in the endosomal membrane while NOD2 is expressed in the cytosol. CpG and MDP together can activate the innate immune system in different cell compartments for complementary stimulation of DCs.[18]

For potent systemic blood cancer vaccines, it is also crucial to efficiently co-deliver Ags and adjuvants to DCs in lymphoid organs for efficient DC stimulation.[8a,19] Prolonged exposure to Ags without the support of adjuvants might lead to immune tolerance.[20] A few novel delivery systems have been developed for anti-AML immunotherapies.[21] However, these platforms were not suitable for delivering cargos to systemic lymphoid compartments, quantitatively co-load TCL and adjuvants, and/or responsively releasing vaccine content in DCs. Previously, we developed intravenously-infused polymersomes based on poly(ethylene glycol)-b-poly(trimethylene carbonate-co-dithiolane trimethylene carbonate)-b-spermine (PEG-P(TMC-DTC)-SP) to targeted deliver protein toxins and/or immunostimulant CpG for efficient cancer cell killing.[22] This polymersome platform is suitable to co-load CpG and TCL which contain diverse proteins to serve as vaccine delivery vehicles.

Here we explored systemic multifunctional nanovaccines that quantitatively co-load dual adjuvants MDP and CpG as well as Ag TCL (MCA-NV) for robust immunotherapy against AML (**Scheme 1**). MCA-NV was designed to mimic the natural structure of bacteria. MDP, a component of the bacteria cell wall, was exposed outside while nucleic acid CpG was loaded inside

of NV. This pseudo-bacteria NV might potently activate innate immunity by engaging multiple types of PRRs simultaneously. Intravenous infusion of varying formulations of NV elicited superior anti-tumor efficacies than subcutaneous injection in both AML- or lymphoma-bearing mice. Dual adjuvant MCA-NV promoted complementary stimulation of DCs and remarkably outperformed single adjuvant NV in upregulating proinflammatory cytokines such as IL-6, TNF-a, and IL-1β. In two orthotopic AML mouse models (MLL-AF9 and WEHI-3), systemic MCA-NV induced robust immune responses to cure 78% of mice and elicited long-term anti-AML immune memory to protect 100% of survived mice from rechallenge of leukemia cells. Furthermore, MCA-NV could serve as prophylactic vaccines to reject engrafted AML cells in healthy mice. This TCL-based systemic NV platform can induce robust and broad immune responses, thus providing a personalized immunotherapeutic strategy to treat various HM.

2. Results

2.1. Preparation and In Vitro Characterization of Nanovaccines

Nanovaccines (NV) co-loading dual adjuvant MDP and CpG and TCL Ag (MCA-NV) were facilely fabricated by self-assembling PEG-P(TMC-DTC)-SP and MDP-PEG-P(TMC-DTC) in buffer containing CpG and TCLs (**Figure** 1A). We functionalized PEG-P(TMC-DTC) with MDP to obtain MDP-PEG-P(TMC-DTC) (Figure S1, Supporting Information).

We induced primary AML in mice by injecting mixed lineage leukemia (MLL-AF9) cells that express a green fluorescent protein (GFP^+ MLL-AF9).[23] Tissues from MLL-AF9 AML mice such as bone marrow/spleen or blood cancer cells (WEHI-3 or A20) were lysed to generate tumor cell lysates (TCLs) which are rich sources of AML-associated antigens (Ag) (Figure 1A; Figure S2, Supporting Information). Both NP40 and RIPA were used as lysis buffers to generate AML cell lysate. On our hands, NP40-generated Ags generally elicited stronger immune responses than that by RIPA and thus NP40 was used in the following experiments unless otherwise indicated.

After NV formation, MDP was located on the surface of MCA-NV while CpG and Ag were loaded into the vesicular interior. We have shown previously that PEG-P(TMC-DTC)-SP is an asymmetric amphiphilic triblock copolymer, which tends to form chimeric polymersomes with PEG segments preferentially at the outer surface while short SP segments at the watery core.[22b,24] To facilitate the alignment of MDP at the outside, the PEG in MDP-PEG-P(TMC-DTC) was designed longer than that in PEG-P(TMC-DTC)-SP ($M_{n\,PEG}$ = 7500 vs 5000 g mol^{-1}). These chimeric polymersomes allow efficient loading of CpG and Ag into the vesicular interior via ionic and hydrogen interactions with SP.

To confirm the vesicular structure and loading of Ag protein and CpG in the interior, we performed fluorescence resonance energy transfer (FRET) experiments. Ag protein and CpG were modified with FITC to form donor Ag^{FITC} and CpG^{FITC}. TRITC was conjugated to spermine in polymer to form an acceptor in the core. The FRET efficiency between Ag^{FITC} and NV^{TRITC} was 35.1% (Figure S3A, Supporting Information). As the average FRET distance was 6.1 nm while the particle size of NV was 56.6 ± 1.3 nm (Figure 1B), Ag^{FITC} must be loaded into the NV core. The FRET efficiency between CpG^{FITC} and NV^{TRITC} was 28.5% and the average FRET distance was 6.4 nm (Figure S3B, Supporting Information), demonstrating that CpG was also encapsulated in the NV inner pocket. The FRET efficiencies obtained were consistent with those reported in the literature for cargo loading in the particles.[25]

With feeding content of CpG and TCL Ag at 4 wt% of polymer, MCA-NV had nearly 100% drug loading efficiency (DLE) for both CpG and Ag (Table S1, Supporting Information). The amount of MDP loaded onto the surface of the polymersomes could also be adjusted by changing the molar ratio of PEG-P(TMC-DTC)-SP and MDP-PEG-P(TMC-DTC) added. Thus, MCA-NVs can achieve quantitative co-loading of TCL Ag and dual adjuvants by simply varying the feeding amount of cargos.

Prepared nanovaccines loading Ag (A-NV), Ag with MDP (MA-NV), and Ag with CpG (CA-NV) exhibited similar size and zeta potential compared to MCA-NVs (Figure 1B; Table S1, Supporting Information). Observation under the transmission electron microscope (TEM) confirmed that MCA-NV had homogeneously spherical morphology with ≈40 nm diameter (Figure 1B). MCA-NV exhibited good colloidal stability against dilution, 10% FBS, and 7-day storage. On the contrary, MCA-NV could be disrupted under acidic conditions and demonstrated accelerated release of cargo at pH 5.0 (Figure 1C,D). Due to the disulfide bond crosslinking in polymersomes, MCA-NV also exhibited responsive-release in the reducing environment. Only ≈20% of CpG was released from MCA-NV in non-reducing environment while over 80% of content was released in the presence of 10 mM GSH within 24 h (Figure 1D).

2.2. MCA-NV Induce Robust Stimulation of BMDCs In Vitro

MCA-NV remarkably promoted the uptake of loaded content by APCs such as DCs and macrophages. After 6 h co-incubation of MCA-NV with APCs, the fluorescence signals of vaccine content appeared in the cytosol of DC2.4 or RAW264.7 (Figure S4, Supporting Information). After adding MCA-NVs for 24 h, a substantial amount of CpG and Ag co-localized in the cytosol while a much lower amount of fluorescence was observed when the equivalent amount of free CpG^{Cy3} and Ag^{FITC} was added (Figure 1E,F).

After endocytosis, MCA-NV effectively stimulated bone marrow-derived dendritic cells (BMDCs) in vitro. The percentage of mature ($CD80^+CD86^+$) BMDCs induced by A-NV was only 27.3% while MA-NV significantly elevated the percentage to 35.4%. Due to the strong stimulating effect of CpG, both CA-NV group and the dual adjuvant group (MCA-NV) had matured BMDCs over 70% (Figure 1G,H). Notably, in comparison to the single adjuvant group CA-NV and MA-NV, dual adjuvant MCA-NV induced significantly higher antigen presentation ability and secretion of proinflammatory cytokines by BMDCs (Figure 1I–L). The amount of tumor necrosis factor-alpha (TNF-α) secreted by BMDCs treated with MCA-NV was 3.4-, 6.8-, and 9.0-fold higher than those by BMDCs treated with CA-NV, MA-NV, and A-NV, respectively. Similarly, dual adjuvant MCA-NV outbeated single

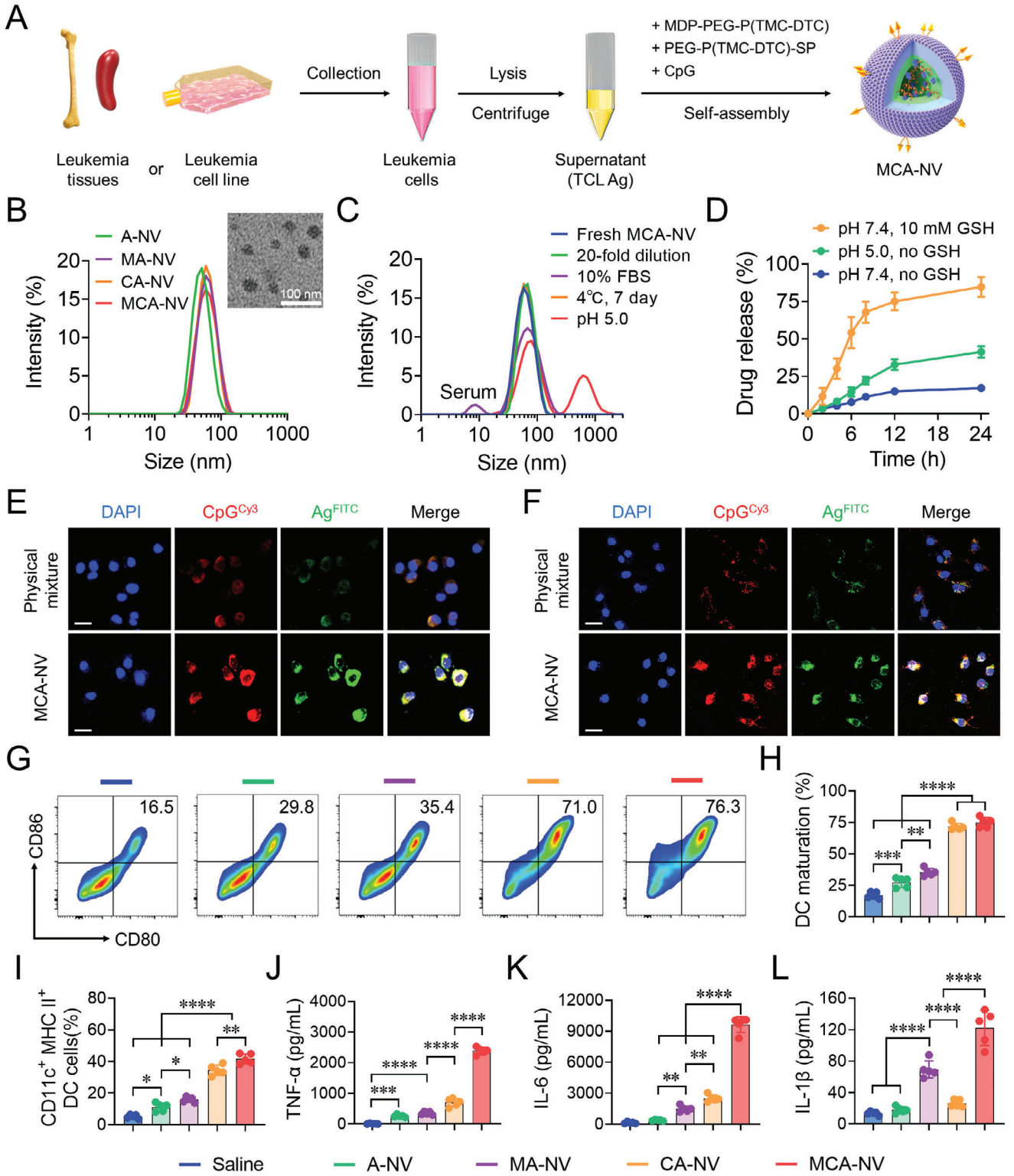

Figure 1. Preparation, characterization, and in vitro immunostimulatory effects of nanovaccines. A) Schematic of MCA-NV preparation to co-load leukemia cell lysate (Ag), CpG, and MDP. B) Size distributions of A-NV, MA-NV, CA-NV and MCA-NV. C) Size change of MCA-NV under different conditions. D) Release kinetics of loaded CpG from MCA-NV in the presence/absence of 10 mM GSH, at pH 7.4 or at pH 5.0 (n = 3). E) Confocal images of DC2.4 cells or F) RAW264.7 cells after pulsing with a physical mixture of free Cy3-labeled CpG (CpG^{Cy3}) and FITC-labeled Ag (Ag^{FITC}), or MCA-NV co-loading equivalent amount of CpG^{Cy3} and Ag^{FITC} for 24 h. Scale bars: 25 μm. (G-L) BMDCs were treated with different formulations of nanovaccines for 24 hrs (n = 5). G) Representative flow cytometry graphs for expression of CD80 and CD86 by BMDCs. H) Quantitative analysis of the percentage of mature BMDCs ($CD11c^+CD80^+CD86^+$). I) Percentage of $CD11c^+MHCII^+$ BMDCs. Level of pro-inflammatory cytokine J) TNF-α, K) IL-6, and L) IL-1β secreted by BMDCs. Statistical analysis was performed via one-way ANOVA with Tukey's post hoc test, $^*p < 0.05$, $^{**}p < 0.01$, $^{***}p < 0.001$, $^{****}p < 0.0001$.

adjuvant CA-NV and MA-NV by inducing BMDCs to secrete 3.9 and 6.5 times higher amounts of interleukin-6 (IL-6), respectively. MDP has been reported to increase the production of interleukin-1β (IL-1β) in DCs and endothelial cells.[26] Compared to A-NV, MA-NV promoted BMDCs to secrete 3.9-fold more IL-1β while CA-NV did not trigger significantly higher IL-1β production than A-NV. Excitingly, dual adjuvant MCA-NV could further elevate BMDCs' IL-1β production 1.8 times higher than MA-NV, leading to an overall 6.9-fold higher than A-NV. These results confirmed that co-delivering MDP and CpG could complementarily enhance antigen presentation and pro-inflammatory cytokine secretion by BMDCs.

2.3. Systemic Infusion of NV Elicits Superior Efficacy than Subcutaneous Injection

The established murine MLL-AF9 AML model was extremely aggressive as GFP$^+$ leukemia cells grew exponentially in mice after initiation. The percentage of leukemia cells in peripheral blood (PB) could increase by over 30% in less than 5 days (Figure S5A,B, Supporting Information). A massive number of MLL-AF9 cells were also detected in bone marrow (BM), spleen, liver, and lungs (Figure S5C,D, Supporting Information). Phenotypically, tumor-bearing mice exhibited typical AML features including pale rather than dark redbones, swollen spleen, and enlarged liver. The weight of spleens and livers also increased remarkably (Figure S5E,F, Supporting Information).

As intravenously (*i.v.*) infused vaccines can generate antitumor immunity in more lymphoid organs than vaccines injected subcutaneously (*s.c.*), we hypothesized that NV (*i.v.*) might have a higher potency than NV (*s.c.*). To quickly explore the effects of administration routes on the efficacies of NV, we prepared single adjuvant NV loading RIPA-lysed Ags and injected just three doses of NV in initial experiments. Compared to saline, subcutaneously (*s.c.*) injected MA-NV only inhibited 30.7% of leukemia cell growth in PB while intravenously (*i.v.*)-infused MA-NV inhibited the proliferation of leukemia cells 15.9-fold more and significantly prolonged the survival of mice (**Figure** 2A–C). Intravenously administered CA-NV also elicited higher, albeit not significantly different, efficacy compared with CA-NV (*s.c.*) (Figure 2A–C), probably due to the already high potency of CA-NV. In mice bearing with A20 lymphoma, the enhanced efficacy of intravenously injected MA-NV was also observed both as prophylactic (Figure S6A–D, Supporting Information) and therapeutic vaccines (Figure S6E–G, Supporting Information).

Next, we evaluated the impacts of administration routes on the full potency of dual-adjuvant NV with five doses. MCA-NV (*i.v.*) substantially outperformed the subcutaneously-infused counterparts by boosting the inhibition rate of leukemia cells in PB from 65.7% to 99.5% and extending the median survival time (MST) from 38 days to 47 days (Figure 2D–F). Due to rapid disease progression and high heterogeneity, AML-bearing mice might show big variations in response to the same treatment. As the systemic application of NV generally induced more robust efficacy than subcutaneously-injected NV, NV were *i.v.* infused for the following experiments.

2.4. Systemic NV Remarkably Enhance Immune Responses Generated in Lymphoid Organs

After intravenous injection for 24 h, NV loading CpG^{Cy3} (C-NV) and NV co-loading MDP and CpG^{Cy3} (MC-NV) efficiently accumulated in lymph nodes (LNs) and the fluorescence signal in LNs was 2.6- and 2.8-fold higher than that of free CpG^{Cy3} (**Figure** 3A,B). We next investigated the immune responses induced by different formulations of NVs. NVs were injected *i.v.* after transplanting MLL-AF9 leukemia cells and immune cells from different organs were analyzed two days after the last dose (Figure 3C). In order to minimize data skewing due to disease-related death and poor condition of saline-treated mice on day 23 onward, only four doses of NV were injected before analysis of NV-induced immune responses. Enhanced LN-targeted delivery of adjuvants and Ags significantly promoted the maturation of LN DCs. MA-NV induced 24% of CD11c$^+$ DC cells to mature (CD80$^+$CD86$^+$) while both CA-NV and MCA-NV elicited >30% (Figure 3D,E). MCA-NV induced a 2.2-fold increase in the percentage of CD8$^+$ T cells in peripheral blood (PB) in comparison to saline and achieved the highest CD8$^+$ T cell percentage among all formulations (Figure 3F,G). Furthermore, in bone marrow (BM), the proportion of CD8$^+$ T cells was only 1.1% from the saline group. Single adjuvant CA-NV and MA-NV boosted the CD8$^+$ T cell percentage to 3.6% and 4.8% respectively while MCA-NV remarkably increased the proportion of CD8$^+$ T cells to 6.7% (Figure 3H,I). The immunostaining of BM also confirmed that MCA-NV induced evidently more CD8$^+$ T cells than other formulations (Figure 3J). More importantly, MCA-NVs also led to the highest portion of activated CD8$^+$CD69$^+$ T cells in BM (Figure 3K).

In addition, NV also generated more functional CD8$^+$ T cells. In spleens, the percentage of TNF-α^+ CD8$^+$ T cells induced by MCA-NV was 8.7- and 5.8-fold higher than that by saline and A-NV (Figure 3L; Figure S7A, Supporting Information). MCA-NV also outperformed all formulations of NV including single adjuvant MA-NV and CA-NV by generating the most Granzyme B-expressing CD8$^+$ T cells (Figure 3M; Figure S7B, Supporting Information). The proportion of CD4$^+$ T cells in PB and BM was also increased by MCA-NV (Figure S8A,B, Supporting Information). Moreover, MCA-NV induced the proliferation of B cells and NK cells in BM, indicating that MCA-NV could potentially enhance humoral and innate immunity to treat AML (Figure S8B, Supporting Information). Thus, intravenously infused MCA-NV allowed the effective generation of immune responses in varying lymphoid organs and PB. These results matched with the observation obtained when treating solid tumors with systemic vaccines.[4,5]

MCA-NV also induced antigen-specific immune responses. By using model protein OVA as Ag, *i.v.* infused O-NV and MCO-NV induced substantial inhibition of subcutaneous B16-OVA tumor (Figure S9A–C, Supporting Information). Splenocytes were then harvested and pulsed with OVA for both ELISPOT and flow cytometry analysis. Compared to saline, O-NV and MCO-NV elicited 11.3- and 21.7-fold elevation in IFN-γ-producing (OVA-specific) T cells in ELISPOT (Figure S9D,E, Supporting Information). In addition, splenocytes from O-NV and MCO-NV groups had 2.3- and 5.3-fold increase in the percentage of CD69$^+$ cells among CD8$^+$ T cells, respectively (Figure S9F,G, Supporting

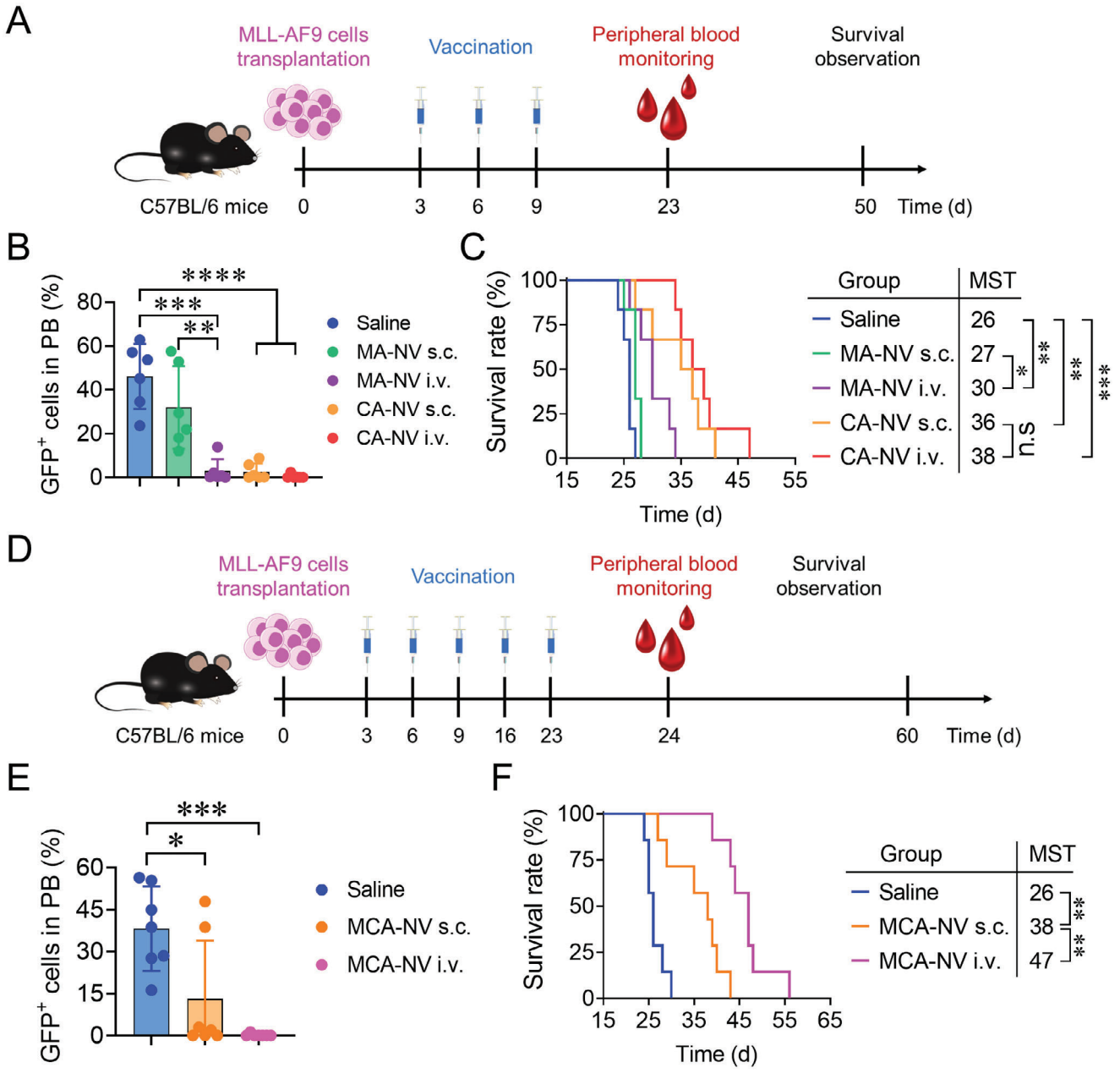

Figure 2. Systemic infusion of NV outperformed subcutaneous injection in treating mice bearing with MLL-AF9 AML. A) Timeline for therapy experiment with single adjuvant NV (MA-NV and CA-NV). B) Percentage of GFP^+ MLL-AF9 cells in peripheral blood (PB) on day 23 (n = 6). C) Survival curve (n = 6). D) Timeline for therapy experiment with dual adjuvant MCA-NV. E) Percentage of GFP^+ MLL-AF9 cells in PB on day 24 (n = 7). F) Survival curve (n = 7). Statistical analysis was performed by one-way ANOVA with Tukey's post hoc test for panels (B), (E) and log-rank test for panels (C), (F), $^*p < 0.05$, $^{**}p < 0.01$, $^{***}p < 0.001$, $^{****}p < 0.0001$.

Information). These results indicated that NV substantially increased the frequency of OVA-specific T cells.

2.5. Systemic NV Eradicate Leukemia Cells in Murine MLL-AF9 Model

We then investigated the anti-AML efficacies of different NV. After loading Ag (generated by NP40 lysis buffer) in NV, five doses of NV were *i.v.* injected after transplantation of MLL-AF9 cells (**Figure** 4A). Due to the aggressive disease progression, the percentage of GFP^+ leukemia cells in PB of saline-treated mice increased exponentially and these mice quickly succumbed to death with a median survival time (MST) of only 27 days (Figure 4B–D). A-NV significantly reduced the proliferation of leukemia cells in PB, while leukemia cells were almost undetectable in CA-NV and MCA-NV groups at 20 days post-leukemia cell transplantation (Figure 4C). A-NV substantially prolonged MST to 49 days

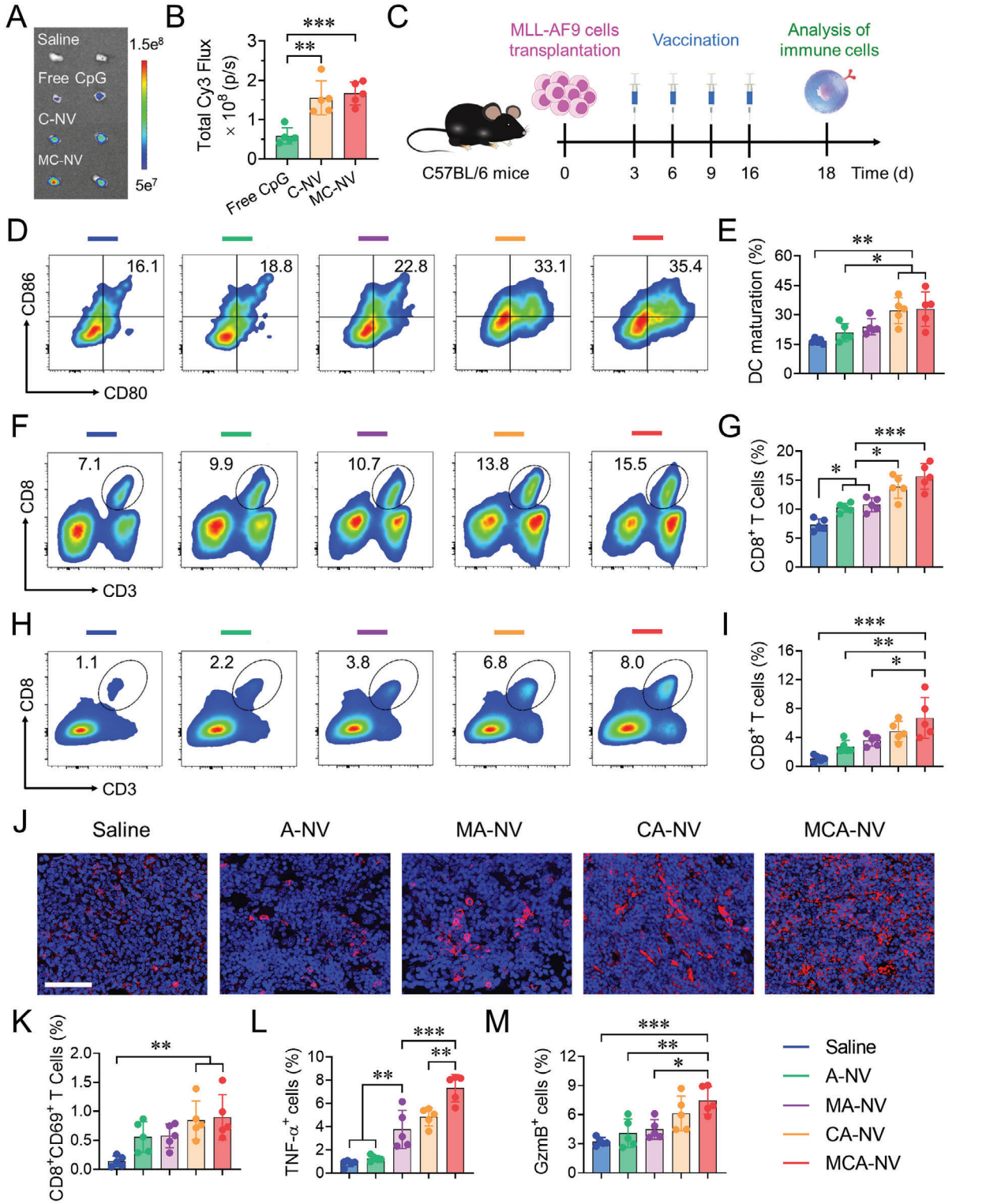

Figure 3. MCA-NV enhanced immune cell activation in vivo. A) Ex vivo fluorescence image and B) quantitative analysis of fluorescence intensity in inguinal lymph nodes (iLNs) 24 h after *i.v.* injection of saline, free CpG, C-NV and MC-NV (n = 5). C) Timeline for analyzing immune responses generated by different formulations of NVs in MLL-AF9 leukemia model (n = 5). D) Representative flow cytometry graphs of CD80 and CD86 expression by DCs and E) percentage of matured ($CD80^+CD86^+$) DCs in iLNs. F) Representative flow cytometry graphs and G) calculated percentages of $CD8^+$ T cells in PB. H) Representative flow cytometry graphs and I) calculated percentages of $CD8^+$ T cells in bone marrow (BM). J) Immunostaining of CD8 in BM sections. Scale bars: 50 µm. K) Calculated percentages of $CD8^+$ T cells expressing early activation marker ($CD69^+$) in BM. Percentages of L) TNF-α and M) Granzyme B expressing $CD8^+$ T cells in spleen. Statistical analysis was performed via one-way ANOVA with Tukey's post hoc test, $^*p < 0.05$, $^{**}p < 0.01$, $^{***}p < 0.001$.

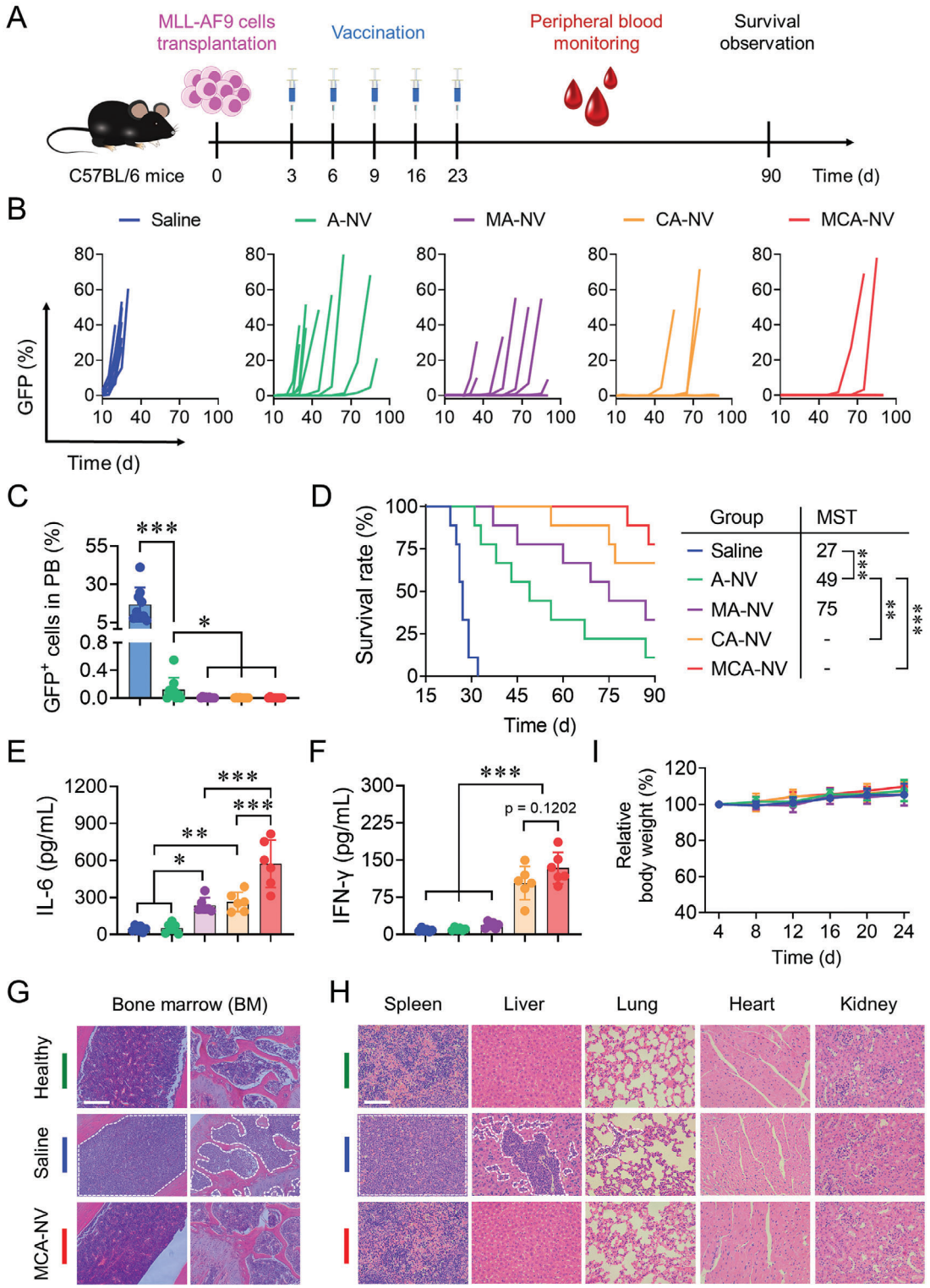

Figure 4. Therapeutic efficacy of MCA-NV in mice bearing with MLL-AF9 AML. A) Timeline for the therapy experiment. Mice bearing with MLL-AF9 leukemia were treated with different formulations of NV. B) Percentage of GFP$^+$ MLL-AF9 cells in PB at different time points (n = 9). C) Percentage of GFP$^+$ MLL-AF9 cells in PB on day 20 (n = 9). D) Survival curve (n = 9). E) Serum concentration of IL-6 and F) IFN-γ on day 25 (n = 6). G) Representative H&E staining images of bone marrow (BM) from healthy mice, AML mice treated with saline and MCA-NV on day 25. Shown are the distribution of hematopoietic cells or leukemia cells in the BM cavity. Scale bars: 100 μm. H) Representative histological images of H&E stained spleen, liver, lung, heart, and kidney on day 25. Scale bars: 50 μm. I) Body weight of mice following different treatments (n = 9). Statistical analysis was performed by one-way ANOVA with Tukey's post hoc test for panels (C,E,F) and log-rank test for panel (D), $^*p < 0.05$, $^{**}p < 0.01$, $^{***}p < 0.001$.

while co-loading MDP and Ags in NV (MA-NV) further increased MST to 75 days with remarkably delayed leukemia cell growth in PB (Figure 4B–D). Dual adjuvant nanovaccine (MCA-NV) cured 78% of mice and yielded a higher survival rate than MA-NV (22%) and CA-NV (67%) at 90 days post MLL-AF9 transplantation (Figure 4B,D).

To assess the efficacy of NV without Ag loading, M-NV, C-NV, and MC-NV were injected *i.v.* after transplantation of MLL-AF9 cells (Figure S10A, Supporting Information). Compared to their respective counterparts loading both Ag and adjuvants (Figure 4D), M-NV, C-NV and MC-NV elicited much weaker anti-AML efficacies and shorter survival of mice (Figure S10B–D, Supporting Information). Compared to MC-NV, MCA-NV also induced a considerable increase in the number of $CD8^+$ T cells in BM (Figure S10E, Supporting Information) as well as the percentage of IFN-γ-expressing and TNF-α-expressing $CD8^+$ T cells in spleen (Figure S10F,G, Supporting Information). Overall, these results indicated that Ags contributed substantially to the therapeutic efficacies of NV.

The enhanced efficacy of dual adjuvant MCA-NV than single adjuvant NV was also observed when Ags were generated by RIPA lysis buffer. Regardless of the quality of TCLs used, dual adjuvant MCA-NV still achieved the highest inhibition rate of leukemia cell growth in PB and prolonged the survival of mice (Figure S11, Supporting Information).

In addition, MCA-NV also synergistically stimulates the production of pro-inflammatory cytokines. MCA-NV induced 2.4- and 2.2-fold higher serum concentrations of IL-6 than single adjuvant nanovaccines MA-NV and CA-NV, respectively (Figure 4E). MCA-NV also induced the highest serum concentration of IFN-γ among all formulations (Figure 4F). Hematoxylin-eosin (H&E)-stained images corroborated that saline-treated mice were burdened with abundant leukemia cells in BM, spleen, and liver, as well as metastatic lesions in the lung. On the contrary, the organs from MCA-NV-treated mice showed similar histology to that of healthy mice, indicating that MCA-NV eradicated leukemia cells (Figure 4G,H). H&E images of all groups of mice demonstrated few leukemia cells in the heart and kidney, similar to what was observed in the literature.[21e,27]

To evaluate the acute toxicity of MCA-NV, we measured the serum levels of pro-inflammatory cytokines just hours post-injection (Figure S12A, Supporting Information). After injection of MA-NV and CA-NV, the serum concentration of IL-6 increased sharply. The dual adjuvant MCA-NV could further raise IL-6 serum concentration to ≈5100 pg mL^{-1} 6 h post injection. This peak value was less than half of the IL-6 triggered by approved Chimeric Antigen Receptor T cells (CAR-T cells) and comparable to CAR-T cells engineered with alleviated cytokine release syndrome (CRS).[28] Notably, the IL-6 concentration quickly dropped 65% by 12 h and back to normal level after 24 h (Figure S12B, Supporting Information). NV-induced IFN-γ exhibited a similar trend (Figure S12C, Supporting Information). No overt body weight loss was observed throughout the time points (Figure S12D, Supporting Information). In addition, all formulations of NV did not significantly change blood cell counts nor trigger differences in H&E analysis of major organs (Figure S13A–C, Supporting Information). Taken together, the moderate CRS triggered by *i.v.* infused MCA-NV was transient and manageable. Therefore, MCA-NV is most likely safe for use.

2.6. Systemic NV Elicit Long-Term Anti-AML Immune Memory

To evaluate the immune memory generated by NVs, we re-challenged cured mice with GFP^+ MLL-AF9 leukemia cells after initial leukemia cell transplantation for 90 days. Healthy mice inoculated with leukemia cells (MLL-AF9 group) or without leukemia cells transplantation (Naive group) both served as controls (**Figure 5A**). The rapid growth of GFP^+ leukemia cells was detected in PB of mice from MLL-AF9 group while negligible GFP^+ cells were detected in the PB of mice previously cured by CA-NV or MCA-NV (Figure 5B). All mice were sacrificed at 20 days post-re-challenge. A substantial number of leukemia cells were found in PB (7.2%), BM (82.6%), spleen (55.2%), liver (36.1%), and lung (2.9%) of MLL-AF9 mice (Figure 5C; Figure S14, Supporting Information). In contrast, NV-elicited immune memory prevented the outgrowth of leukemia cells in these major organs (Figure 5C; Figure S14, Supporting Information). Due to the excessive number of leukemia cells in spleens, mice from MLL-AF9 group had swollen spleens, a classic feature of AML (Figure 5D). The spleens of NV-cured mice were only slightly enlarged in comparison with healthy controls. As leukemia cells were not detected in NV-cured mice by flow cytometry, we reasoned that the minute splenomegaly might be due to immune activation.[29]

NV-treatment increased the percentage of $CD8^+$ effector memory T cells (T_{EM}, $CD44^+CD62L^-$) among T cells in BM by 3.8-fold higher than that in mice from the naive group (Figure 5E,F). Surprisingly, the percentage of $CD8^+$ T_{EM} from MLL-AF9 mice was higher than that from NV-treated mice. A closer look at the data revealed that the excessive growth of leukemia cells in BM rendered too few number and abnormal phenotype of T cells for accurate analysis of memory responses in BM. In the spleen, MCA-NV and CA-NV induced significantly more $CD8^+$ T_{EM} (1.7–2.1-fold higher) than naive or MLL-AF9-bearing mice. In PB, NV-cured mice also had higher $CD8^+$ T_{EM} than naive and MLL-AF9 groups (Figure 5E,F). In addition, more $CD4^+$ T_{EM} was also detected in BM, spleen, and PB in the NV-treated groups, indicating successful generation of immune memory by NVs (Figure S15, Supporting Information). Furthermore, we also observed stronger stimulation of DCs in LNs. The percentage of mature DCs among $CD11c^+$ cells in MCA-NV-treated mice was significantly higher than that in CA-NV, MLL-AF9, and naive groups (Figure S16, Supporting Information).

In order to verify that leukemia cells were indeed absent in mice instead of being merely below the detection limit of the flow cytometer, we collected BM cells from MLL-AF9 or NV-treated mice and then transplanted them *i.v.* into healthy recipient mice (secondary transplantation). Before the secondary transplantation of BM cells, sublethal irradiation was conducted to weaken the immune system of the recipient mice to facilitate the transplantation of donor cells from NV-cured mice.[21c,30] As just a few transferred MLL-AF9 leukemia stem cells (LSCs) were able to induce leukemia in the recipient mice,[23] the secondary transplantation could be an effective method to detect residual AML cells that could be overlooked by flow cytometry. Due to the presence of a large amount of leukemia cells in BM from MLL-AF9 mice, engraftment of BM cells from MLL-AF9 group quickly appeared in the PB of recipient mice after secondary transplantation and caused death of mice. However, all mice that received

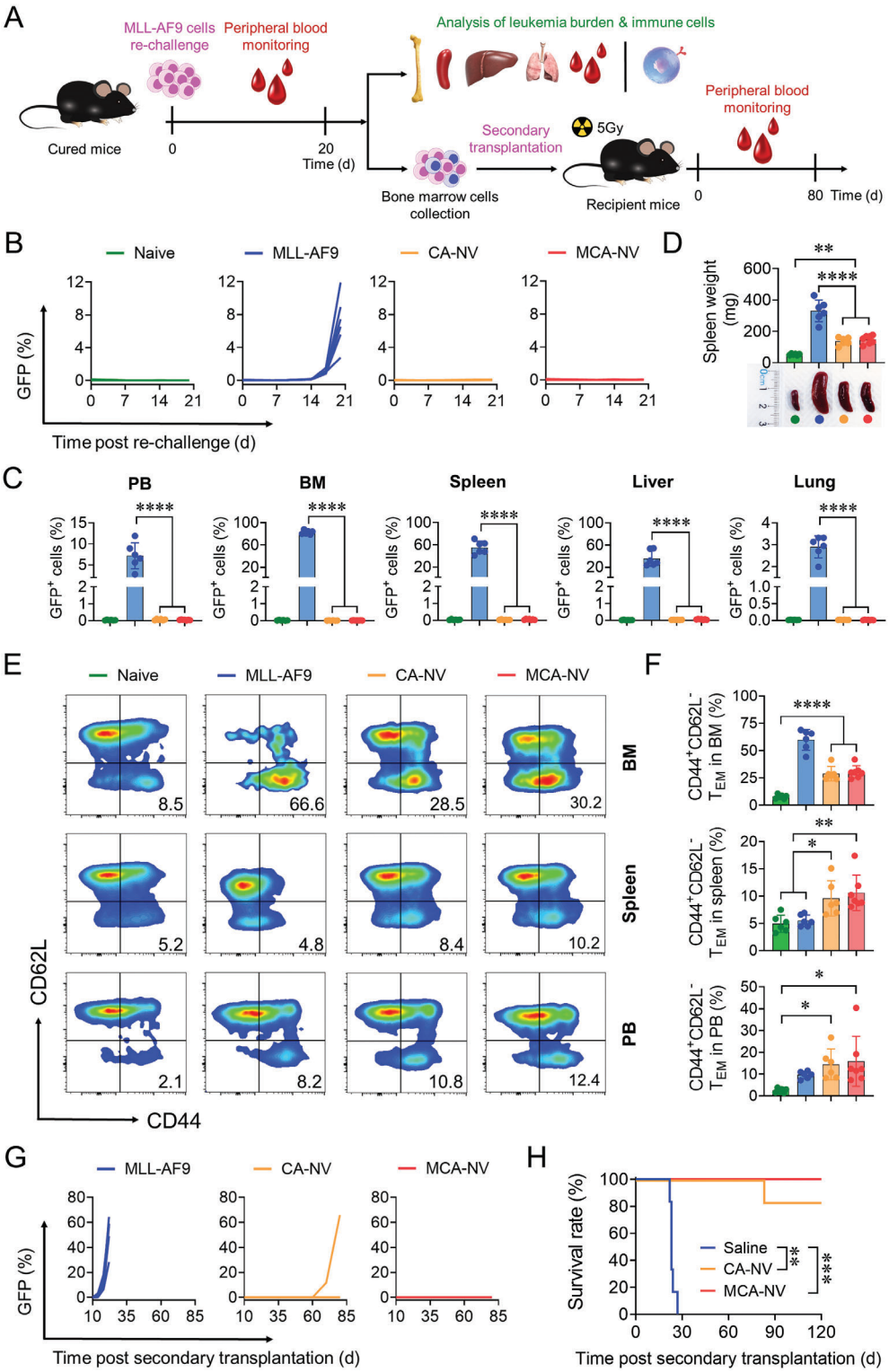

Figure 5. MCA-NV elicited immune memory to prevent recurrence due to rechallenged leukemia cells. A) Timeline for the rechallenge experiment. B) Percentage of GFP^+ leukemia cells progression in PB post-re-challenge (for Naive, MLL-AF9, and CA-NV group: n = 6; for MCA-NV group: n = 7). C) Percentage of GFP^+ leukemia cells engraftment in different organs on day 20 post re-challenge. D) Morphology and weight of spleens from mice in different groups. Scale bars: 1 cm. E) Representative flow cytometry graphs and F) percentage of T_{EM} cells ($CD44^+CD62L^-$) among $CD3^+CD8^+$ T cells in BM, spleen, and PB on day 20 post-re-challenge. G) GFP^+ leukemia cells progression in PB post-secondary transplantation. (H) Survival curve. Statistical analysis was performed by one-way ANOVA with Tukey's post hoc test for panels (C,D,F) and log-rank test for panel (H), $^*p < 0.05$, $^{**}p < 0.01$, $^{***}p < 0.001$, $^{****}p < 0.0001$.

BM cells from MCA-NV-cured mice were free of leukemia cells in PB even after 80 days post-secondary transplantation and survived. This indicates that MCA-NV induced effective anti-AML immune memory and no leukemia cells were present in BM after MCA-NV treatment (Figure 5G,H).

2.7. Systemic NV Demonstrate Promising Efficacy in Mice with WEHI-3 AML

We also investigated the therapeutic efficacies of different NV in WEHI-3 murine AML model (**Figure 6A**). WEHI-3-Luc leukemia cells grew rapidly in mice treated with saline, leading to a rapid increase in the bioluminescence signals and short MST at 52 days. A-NV significantly prolonged the MST to 77 days and MA-NV could further increase the MST of mice to 108 days (Figure 6B–D). Both CA-NV and MCA-NV substantially delayed the outgrowth of WEHI-3-Luc cells. After leukemia cell transplantation for 300 days, the survival rate of CA-NV-treated and MCA-NV-treated mice was 56% and 78%, respectively (Figure 6B–D). Notably, not only did MCA-NV inhibit the growth of leukemia cells most efficiently, but MCA-NV also significantly enhanced the production of pro-inflammatory cytokines (Figure 6E–G). As opposed to MA-NV, MCA-NV elicited 2.0, 4.5, and 1.5-fold higher concentrations of TNF-α, IFN-γ and IL-1β in serum. Even in comparison to CA-NV, MCA-NV induced 1.5, 1.5, and 2.4-fold elevation in serum TNF-α, IFN-γ and IL-1β. Furthermore, MCA-NV also yielded higher secretion of IL-6 than all other formulations (Figure 6H). Thus, NV co-loading TCL and dual adjuvants (MCA-NV), demonstrated the most potent efficacy among all formulations when treating WEHI-3 AML.

2.8. Prophylactic Systemic NV Protect Mice Against AML

Next, we evaluated the efficacy of MCA-NV as a prophylactic vaccine for AML. Mice were immunized with three doses of MCA-NV before inoculation with varying amounts of GFP$^+$ MLL-AF9 leukemia cells (**Figure 7A**). MCA-NV substantially delayed the growth of leukemia cells in PB when 5×10^5 MLL-AF9 cells were transplanted (Figure 7B,C) and increased the proportion of CD8$^+$ T cells in PB 1.3-times higher than that in saline-treated control groups (Figure 7D,E). Even when the number of MLL-AF9 cells transplanted was raised tenfold to 5×10^6 cells per mouse, MCA-NV still could considerably delay the growth of leukemia cells (Figure 7B). At 20 days post 5×10^6 MLL-AF9 cells transplantation, the average percentage of GFP$^+$ leukemia cells in PB of saline-treated mice was 40.1% while that in mice immunized with MCA-NV was only 1.7% (Figure 7C). The percentage of CD8$^+$ T cells was also increased 1.6-fold higher (Figure 7D,E). Mice without treatment quickly succumbed to AML (MST 28 days) while MCA-NV significantly improved the MST of mice to 52 days. Even 75 days post MLL-AF9 cells transplantation, 43% of MCA-NV immunized mice were still alive. When mice were transplanted with tenfold more MLL-AF9 cells (5×10^6 cells per mouse), MCA-NV immunization still could prolong MST from 23 to 37 days (Figure 7F). MCA-NV did not cause overt body weight change and implied the treatments were safe as a prophylactic vaccine for AML (Figure 7G). Thus, MCA-NV could offer strong and lasting protective effects to prevent the initial onset of AML.

3. Discussion

Hematological malignancies, a collection of blood neoplasias such as leukemia, lymphoma, and multiple myeloma, had an estimated 1.3 million new cases and accounted for >7% of cancer deaths worldwide in 2020.[4,31] Despite the encouraging efficacy of cancer vaccines shown in solid tumor treatment, the potency of cancer vaccines against blood cancer is still mediocre,[3] partly owing to insufficient stimulation of dendritic cells (DCs) in the body and lacking appropriate tumor antigens (Ags). As AML is the most difficult-to-treat hematological malignancy (HM), exploring effective cancer vaccines for AML is of great clinical and socio-economic interests and can shed insight into developing immunotherapies to other types of HM.

In this study, we explored systemic vaccines for blood cancers. We developed potent systemic MCA-NV to efficiently co-deliver TCL as Ags and dual adjuvants MDP and CpG for eliciting robust and broad immune responses against AML. MCA-NV cured 78% of mice in both MLL-AF9 and WEHI-3 AML models. The two models were relatively difficult to treat as combinations of immune checkpoint inhibitors (ICIs) only elicited slight survival benefits (Figure S17, Supporting Information). Systemic NV also boosted the therapeutic efficacy of lymphoma (Figure S6, Supporting Information), indicating this approach could be generalized to enhance the prognosis of different types of HM. More importantly, MCA-NV induced strong and lasting immune memory to protect mice from both recurrences or initial outgrowth of leukemia cells.

We reasoned the intravenous administration route contributed remarkably to the superior efficacies of NV. Compared to subcutaneous injection, systemic administration substantially enhanced efficacy for all NV formulations tested in both leukemia and lymphoma models (Figure 2; Figure S6, Supporting Information). Intravenously-infused MCA-NV generated body-wide anti-AML immunity and memory responses in LNs, spleen, bone marrow, and PB (Figure 5E,F; Figures S15 and S16, Supporting Information). As blood cancer cells usually accumulate in these locations, systemic NV might mediate more direct and efficient killing of tumor cells. Recent research findings in solid tumor treatment also corroborated our observations. Much enhanced efficacies of intravenously-infused cancer vaccines, in comparison to the same vaccines injected subcutaneously, were reported in multiple murine solid tumor models.[6a–e] Furthermore, systemic cancer vaccines were shown to induce T cells with more stem-like phenotype and higher tumor-killing ability.[6a,b,d]

The robust efficacy of NV might also be attributed to their ability to quantitatively co-load and efficiently co-deliver Ag and dual adjuvant for promoting DC stimulation. As reacting through the amino group of MDP caused minimal impairment on NOD2-stimulating effects of MDP,[32] we chemically linked MDP to NH_2-functionalized PEG-P(TMC-DTC) polymer via 2-aminoethanethiol. As MDP-PEG-P(TMC-DTC) and CpG could be quantitatively incorporated into NV, tailoring the feeding amount of the two allowed precise tuning of the ratio between

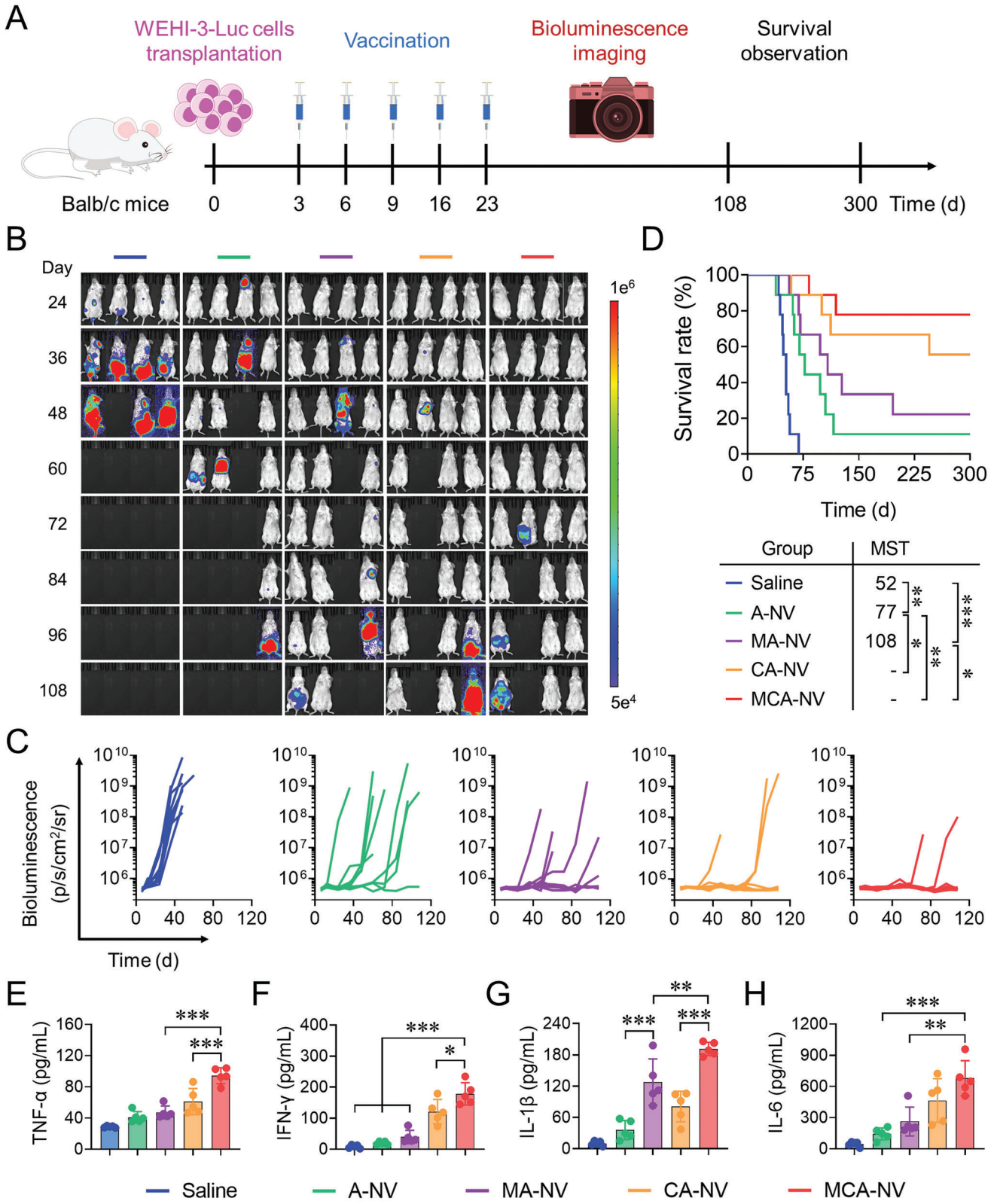

Figure 6. Therapeutic efficacy of nanovaccines in WEHI-3 AML model. A) Timeline for therapy experiment. B) Representative bioluminescence IVIS image and C) bioluminescence intensity at different time points (n = 9). D) Survival of the mice from different treatment groups (n = 9). Serum levels of pro-inflammatory cytokine E) TNF-α, F) IFN-γ, G) IL-1β, and H) IL-6 on day 25 (n = 5). Statistical analysis was performed by one-way ANOVA with Tukey's post hoc test for panels (E–H) and log-rank test for panel (D), $^{*}p < 0.05$, $^{**}p < 0.01$, $^{***}p < 0.001$.

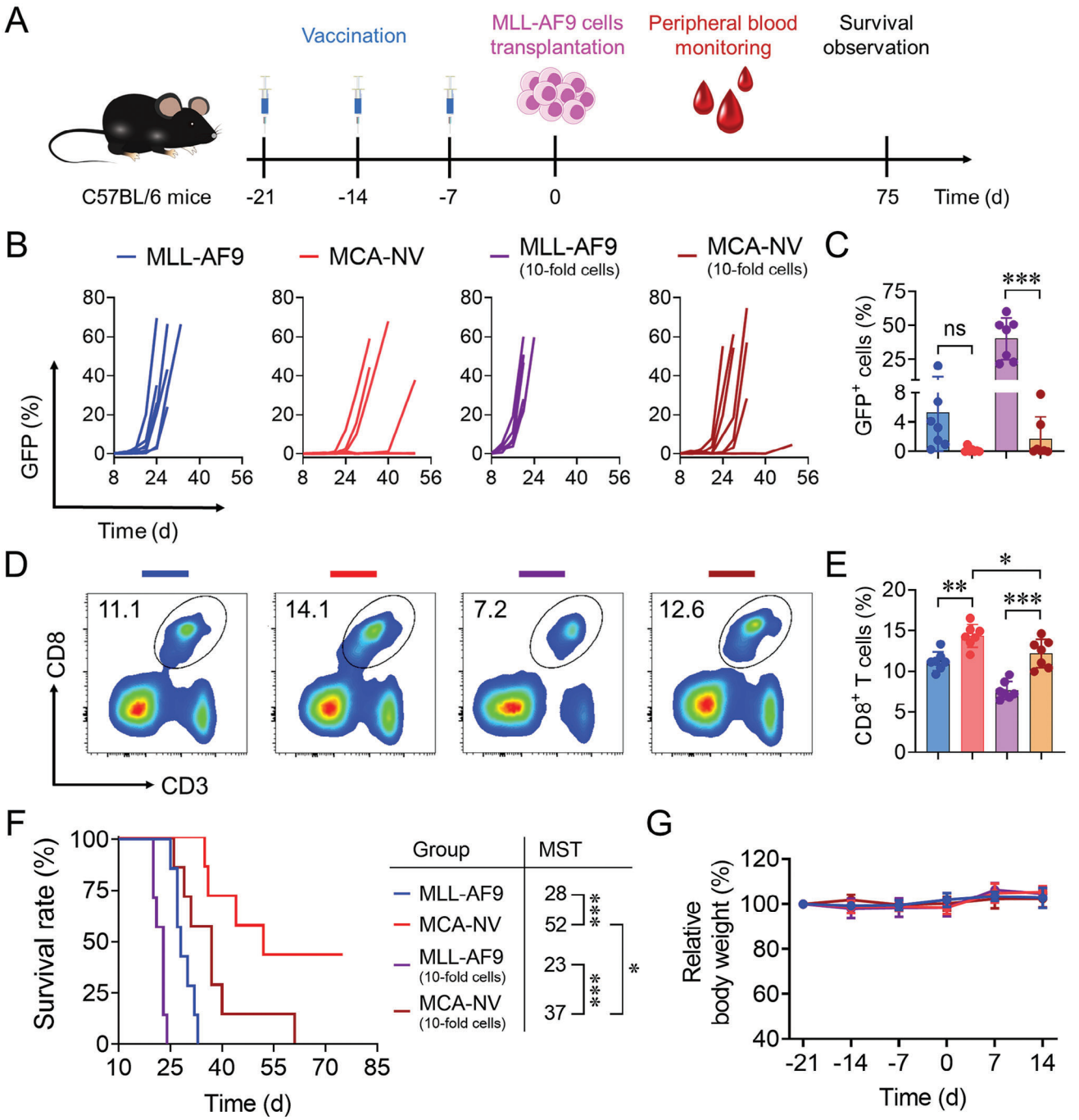

Figure 7. MCA-NV could serve as a protective vaccine for AML. A) Timeline for the experiment. B) Percentage of GFP+ MLL-AF9 leukemia cells in PB at different time points (n = 7). C) Percentage of GFP+ MLL-AF9 leukemia cells in PB at 20 days post-transplantation (n = 7). D) Representative flow cytometric graphs and E) percentage of CD8+ T cells in PB at 20 days post-transplantation (n = 7). F) Survival of mice in different treatment groups v (n = 7). G) Body weight of mice following different treatments (n = 7). Statistical analysis was performed by one-way ANOVA with Tukey's post hoc test for panels (C), (E) and log-rank test for panel (F), $^{*}p < 0.05$, $^{**}p < 0.01$, $^{***}p < 0.001$.

two adjuvants to obtain optimal DC stimulation. By activating both NOD2 and TLR9 signaling pathways,[14b,33] dual adjuvant MCA-NV can induce complementary stimulation of DCs. Indeed, compared to single-adjuvant NV (MA-NV and CA-NV), dual-adjuvant MCA-NV achieved the highest anti-AML efficacies among all formulations. Despite the fact that CpG seemed to play a more dominant role in the efficacy, dual-adjuvant MCA-NV yielded an obvious increase in cure rate and fewer residual leukemia cells in BM than CA-NV (Figures 4D and 5G,H). Furthermore, in comparison to CA-NV, MCA-NV induced strikingly higher secretion of pro-inflammatory cytokine by BMDCs in vitro (Figure 1J–L), generated significantly more TNF-α

expressing $CD8^+$ T cells in the spleen (Figure 3L), and elicited substantial higher serum concentration of IL-6 (≈2.2-fold higher) (Figure 4E). Therefore, it is important to have dual adjuvant as MDP could further improve the efficacy of CA-NV. In addition, MCA-NV were stabilized by disulfide-crosslinking between constituting polymers to minimize leakage of Ags and CpG in circulation, thus increasing the bioavailability of cargo. Furthermore, once MCA-NV were internalized by DCs, the reduction-sensitive MCA-NV could responsively release vaccine content for optimal DC stimulation.

Employing TCL as Ags enabled MCA-NV to generate broad and yet personalized anti-AML immune responses. Since leukemia cell lysate contains a wide range of TAAs and neoantigens for AML, MCA-NV can induce immunity to minimize the immune escape of leukemia cells. MCA-NV can be used for all patients regardless of their AML subtypes and remarkably reduces the chances of relapse. In addition, leukemia cells are readily available in blood or bone marrow, facilitating the generation of TCL. Using TCL as Ags can also circumvent the technically challenging, time-consuming, and expensive procedures to identify and synthesize relevant neoantigens.[2a]

To further enhance therapeutic efficacy, combination therapy is a viable option. Induction chemotherapies usually elicit apparent remission of AML, but suffer from high replace rates due to the outgrowth of residual AML cells.[7d] Chimeric antigen receptor T (CAR-T) cell therapies or antibodies targeting a particular subtype of AML or subpopulation of AML cells elicited promising efficacies, but the residual drug-untargetable AML cells might still lead to frequent relapses and high mortality.[34] Given their potential to trigger broad and robust immune responses, systemic MCA-NV can complement the existing treatment options to eliminate minimal residual disease or serve as a standalone therapy. As ICIs could help vaccine-induced T cells to counter immunosuppression,[35] the anti-tumor efficacy of MCA-NV might be further improved with the support of ICIs.

MCA-NV might also have the potential to treat acute lymphoid leukemia (ALL). Despite the promising efficacy of CAR-T cell therapy to B-cell ALL, relapse due to residual cells still occurs. Furthermore, T-cell ALL is still intractable. MCA-NV might trigger broad anti-ALL immune responses to complement other immunotherapies or even act as a standalone treatment option.

4. Conclusion

In summary, we developed multifunctional systemic nanovaccine MCA-NV for intractable blood cancers. Intravenously infused MCA-NV could efficiently co-deliver TCL and adjuvant CpG and MDP to lymphoid DCs for robust and personalized immunotherapy against AML, the most difficult-to-treat HM. Dual adjuvants loaded in NV simultaneously stimulated NOD2 and TLR9 signaling pathways for complementary activation of DCs and significantly elevated the secretion of pro-inflammatory cytokines by DCs. MCA-NV cured ≈80% of mice in multiple AML models and elicited long-term immune memory to protect 100% of cured mice from leukemia cell rechallenge. In addition, systemic NV also enhanced the efficacies of lymphoma, indicating that the platform is applicable to treat varying types of HM. By employing TCL as Ags, MCA-NV might minimize the immune escape of cancer cells to reduce relapse due to residual tumor cells and offer personalized immunotherapy to HM patients. Overall, MCA-NV provides a potent and versatile platform to efficiently treat HM and might shed insights into designing next-generation vaccines for blood cancers.

5. Experimental Section

Cells, Animals, and AML Models: Six-week-old female C57BL/6 mice (Beijing Charles River Laboratory Animal Technology Co., Ltd.) and 6-week-old female Balb/c mice (Shanghai Jihui Laboratory Animal Care Co., Ltd) were housed in pathogen-free conditions at the Soochow University. All animal experiments were approved by the Animal Care and Use Committee of Soochow University, and all protocols of animal studies conformed to the Guide for the Care and Use of Laboratory Animals (202211A0108, 202303A0879).

GFP^+ MLL-AF9 primary AML cells, WEHI-3-Luc AML cell line, and A20-Luc lymphoma cell line were kindly provided by Tianhui Liu (The First Affiliated Hospital of Soochow University). B16-OVA cells were kindly provided by Yiran Zheng (College of Pharmaceutical Sciences of Soochow University). WEHI-3-Luc or A20-Luc cells were cultured in DMEM medium containing 10% FBS, 100 μg mL^{-1} streptomycin, 100 IU mL^{-1} penicillin, and anti-mycoplasma reagent. B16-OVA cells were cultured in RPMI-1640 medium containing 10% FBS, 100 μg mL^{-1} streptomycin, 100 IU mL^{-1} penicillin, and anti-mycoplasma reagent. MLL-AF9 AML model was established by tail vein injection of 5×10^5 GFP^+ MLL-AF9 cells into each C57BL/6 mouse. WEHI-3 AML model was established via tail vein injection of 5×10^6 WEHI-3-Luc cells into Balb/c mice, A20 lymphoma model was established via tail vein injection of 1×10^7 A20-Luc cells into Balb/c mice.

Preparation and Characterization of MCA-NV: MCA-NV were fabricated by solvent exchange method. Briefly, 100 μL of DMF solution of PEG-P(TMC-DTC)-SP /MDP-PEG-P(TMC-DTC) (concentration: 40 mg mL^{-1}, molar ratio: 1/1) was added into 900 μL of HEPES buffer containing CpG and Ag (10 mM, pH 6.8, theoretical CpG and Ag loading content: 4 wt%). After stirring for 10 min at 37 °C, the sample was dialyzed (MWCO: 1000 kDa) sequentially against HEPES (10 mM, pH 6.8) for 3 h, and PB (10 mM, pH 7.4) for 3 h with an exchange of fresh medium every hour., A-NV, MA-NV, and CA-NV were prepared similarly with corresponding components.

The size distribution of NV was determined by dynamic light scattering (DLS, Zetasizer Nano-ZS, Malvern). The Zeta potential of NVs was measured at 25 °C using a Zetasizer Nano-ZS. The morphology of MCA-NV was characterized by Transmission electron microscope (TEM, FEI Tecnai G220). MCA-NV sample was prepared by dropping 10 μL of polymersome suspension (1 mg mL^{-1}) on the copper grid followed by staining with 1 wt.% phosphotungstic acid.

Fluorescence resonance energy transfer (FRET) analysis was performed to evaluate the location of Ag (or CpG) in NV after loading. Ag and CpG were labeled with FITC (Ag^{FITC} and CpG^{FITC}) while TRITC was conjugated to spermine in polymer PEG-P(TMC-DTC)-SP. Ag^{FITC} and PEG-P(TMC-DTC)-SP-TRITC were mixed and allowed for NV formation. NV^{TRITC} loading Ag^{FITC} (Ag^{FITC}-NV^{TRITC}), Ag^{FITC}, and NV^{TRITC} were excited at wavelength 440 nm, and their emission spectrum was recorded by using a plate reader. The distance between FRET pairs (R) and FRET efficiency (E) was calculated by the following equations. The R and E were also calculated for CpG^{FITC}-NV^{TRITC}. F_{DA} is the fluorescence intensity when the acceptor is present; F_D is the fluorescence intensity when the acceptor is absent; R_0 is the Förster distance at 50% transfer efficiency and R_0 is 5.5 nm for FITC-TRITC.

$$E = 1 - \frac{F_{DA}}{F_D},\ R = R_0 \sqrt[6]{\frac{1}{E} - 1} \quad (1)$$

CpG and Ag loading were measured by NanoDrop (Thermo Scientific) and BCA protein assay kit, respectively. The drug loading efficiency (DLE) or content (DLC) was calculated according to the following equations:

$$\text{DLC (wt.\%)} = \frac{\text{weight of loaded CpG or Ag}}{\text{total weight of polymers and loaded CpG or Ag}} \times 100 \quad (2)$$

$$\text{DLE (\%)} = \frac{\text{weight of loaded CpG or Ag}}{\text{weight of CpG or Ag in feed}} \times 100 \quad (3)$$

The colloidal stability of MCA-NV against 20-fold dilution with PB, overnight incubation with 10% FBS (37 °C, 100 rpm), storage (4 °C, 7 days), and acidic environment (pH 5.0) was monitored by DLS. In vitro release kinetics of Cy3-labeled CpG (CpG-Cy3) from MCA-NV was analyzed in PB (10 mM, pH 7.4) with or without 10 mM GSH and PB (10 mM, pH 5.0) (n = 3). In brief, 0.5 mL of MCA-NV (CpG concentration: 50 μg mL^{-1}) was added into a dialysis bag (Spectra/Pore, MWCO 1000 kDa) submerged in 25 mL of reservoir medium with shaking at 100 rpm at 37 °C. At different time points, 5 mL of dialysate was taken out and then 5 mL of fresh medium was added. The sampled dialysate was lyophilized and redissolved in 200 μL DMSO. The fluorescence of the sample solution was measured by a multifunctional microplate reader (Thermo Varioskan LUX).

Statistical Analysis: The data were presented as mean ± SD and analyzed by Prism 8.1. Comparisons between multiple groups were analyzed by one-way ANOVA with Tukey post-test unless otherwise indicated. Comparison between the two groups was done by a two-tailed paired Student *t*-test. Kaplan–Meier survival curves were analyzed by log-rank test. $^{*}p < 0.05$, $^{**}p < 0.01$, $^{***}p < 0.001$ and $^{****}p < 0.0001$.

Supporting Information

Supporting Information is available from the Wiley Online Library or from the author.

Acknowledgements

This work was financially supported by the National Natural Science Foundation of China (52233007), the National Key R&D Program of China (2021YFB3800900, 2022YFA1206002, 2022YFC2502700), Excellent Youth Science Fund of Jiangsu Province (BK20211553), Translational Research Grant of NCRCH (2021ZKMB01), "Open Competition to Select the Best Candidates" Key Technology Program for Cell Therapy of NCTIB (NCTIB2023XB02012), Interdisciplinary Basic Frontier Innovation Program of Suzhou Medical College of Soochow University (YXY2301005) and Priority Academic Program Development (PAPD) of Jiangsu Higher Education Institutions.

Conflict of Interest

The authors declare no conflict of interest.

Author Contributions

P.Z., T.W., and G.C. contributed equally to this work. Z.Z., Y.Z., P.Z., G.C., and L.T. conceived and designed the experiments. P.Z., T.W., G.C., R.Y., and W. Wan performed the experiments. P.Z. and T.W. analyzed and processed the data. All authors participated in the discussion of the results and made comments on the manuscript. Y.Z. and P.Z. wrote the initial manuscript. P.Z., Y.Z., Z.Z., and T.L. further revised the manuscript.

Data Availability Statement

The data that support the findings of this study are available from the corresponding author upon reasonable request.

Keywords

acute myeloid leukemia, cancer immunotherapy, intracellular codelivery of antigens and adjuvants, nanovaccine, personalized vaccine

Received: May 20, 2024
Revised: June 30, 2024
Published online: August 22, 2024

[1] a) L. A. Rojas, Z. Sethna, K. C. Soares, C. Olcese, N. Pang, E. Patterson, J. Lihm, N. Ceglia, P. Guasp, A. Chu, R. Yu, A. K. Chandra, T. Waters, J. Ruan, M. Amisaki, A. Zebboudj, Z. Odgerel, G. Payne, E. Derhovanessian, F. Müller, I. Rhee, M. Yadav, A. Dobrin, M. Sadelain, M. Łuksza, N. Cohen, L. Tang, O. Basturk, M. Gönen, S. Katz, et al., *Nature* **2023**, *618*, 144; b) G. Cafri, J. J. Gartner, T. Zaks, K. Hopson, N. Levin, B. C. Paria, M. R. Parkhurst, R. Yossef, F. J. Lowery, M. S. Jafferji, T. D. Prickett, S. L. Goff, C. T. McGowan, S. Seitter, M. L. Shindorf, A. Parikh, P. D. Chatani, P. F. Robbins, S. A. Rosenberg, *J. Clin. Invest.* **2020**, *130*, 5976.

[2] a) M. J. Lin, J. Svensson-Arvelund, G. S. Lubitz, A. Marabelle, I. Melero, B. D. Brown, J. D. Brody, *Nat Cancer* **2022**, *3*, 911; b) M. Saxena, S. H. van der Burg, C. J. M. Melief, N. Bhardwaj, *Nat. Rev. Cancer* **2021**, *21*, 360.

[3] a) M. Yamaguchi, N. Takezako, T. Kiguchi, S. Miyawaki, Y. Heike, K. Mitsuki, T. Yoshida, E. L. Liew, T. Naoe, *Blood* **2018**, *132*, 29; b) P. G. Maslak, T. Dao, Y. Bernal, S. M. Chanel, R. Zhang, M. Frattini, T. Rosenblat, J. G. Jurcic, R. J. Brentjens, M. E. Arcila, R. Rampal, J. H. Park, D. Douer, L. Katz, N. Sarlis, M. S. Tallman, D. A. Scheinberg, *Blood Adv* **2018**, *2*, 224; c) L. Biavati, C. A. Huff, A. Ferguson, A. Sidorski, M. A. Stevens, L. Rudraraju, C. Zucchinetti, S. A. Ali, P. Imus, C. B. Gocke, R. M. Gittelman, S. Johnson, C. Sanders, M. Vignali, A. Gandhi, X. Ye, K. A. Noonan, I. Borrello, *Clin. Cancer Res.* **2021**, *27*, 6696.

[4] L. Tang, Z. Huang, H. Mei, Y. Hu, *Signal Transduct* **2023**, *8*, 306.

[5] a) L. M. Kranz, M. Diken, H. Haas, S. Kreiter, C. Loquai, K. C. Reuter, M. Meng, D. Fritz, F. Vascotto, H. Hefesha, C. Grunwitz, M. Vormehr, Y. Hüsemann, A. Selmi, A. N. Kuhn, J. Buck, E. Derhovanessian, R. Rae, S. Attig, J. Diekmann, R. A. Jabulowsky, S. Heesch, J. Hassel, P. Langguth, S. Grabbe, C. Huber, Ö. Türeci, U. Sahin, *Nature* **2016**, *534*, 396; b) K. Reinhard, B. Rengstl, P. Oehm, K. Michel, A. Billmeier, N. Hayduk, O. Klein, K. Kuna, Y. Ouchan, S. Wöll, E. Christ, D. Weber, M. Suchan, T. Bukur, M. Birtel, V. Jahndel, K. Mroz, K. Hobohm, L. Kranz, M. Diken, K. Kühlcke, Ö. Türeci, U. Sahin, *Science* **2020**, *367*, 446.

[6] a) F. Baharom, R. A. Ramirez-Valdez, K. K. S. Tobin, H. Yamane, C.-A. Dutertre, A. Khalilnezhad, G. V. Reynoso, V. L. Coble, G. M. Lynn, M. P. Mulè, A. J. Martins, J. P. Finnigan, X. M. Zhang, J. A. Hamerman, N. Bhardwaj, J. S. Tsang, H. D. Hickman, F. Ginhoux, A. S. Ishizuka, R. A. Seder, *Nat. Immunol.* **2021**, *22*, 41; b) F. Baharom, R. A. Ramirez-Valdez, A. Khalilnezhad, S. Khalilnezhad, M. Dillon, D. Hermans, S. Fussell, K. K. S. Tobin, C. A. Dutertre, G. M. Lynn, S. Müller, F. Ginhoux, A. S. Ishizuka, R. A. Seder, *Cell* **2022**, *185*, 4317; c) X. Sun, Y. Zhang, J. Li, K. S. Park, K. Han, X. Zhou, Y. Xu, J. Nam, J. Xu, X. Shi, L. Wei, Y. L. Lei, J. J. Moon, *Nat. Nanotechnol.* **2021**, *16*, 1260; d) G. M. Lynn, C. Sedlik, F. Baharom, Y. Zhu, R. A. Ramirez-Valdez, V. L. Coble, K. Tobin, S. R. Nichols, Y. Itzkowitz, N. Zaidi, J. M. Gammon, N. J. Blobel, J. Denizeau, P. de la Rochere, B. J. Francica, B. Decker, M. Maciejewski, J. Cheung, H. Yamane, M. G. Smelkinson, J. R. Francica, R. Laga, J. D. Bernstock, L. W. Seymour, C. G. Drake, C. M. Jewell, O. Lantz, E. Piaggio, A. S. Ishizuka, R. A. Seder, *Nat. Biotechnol.* **2020**, *38*, 320; e) C. Grunwitz, N. Salomon, F. Vascotto, A. Selmi, T. Bukur, M. Diken, S. Kreiter, Ö. Türeci, U. Sahin, *Oncoimmunology*

2019, *8*, e1629259; f) P. J. DeMaria, K. Lee-Wisdom, R. N. Donahue, R. A. Madan, F. Karzai, A. Schwab, C. Palena, C. Jochems, C. Floudas, J. Strauss, J. L. Marté, J. M. Redman, E. Dombi, B. Widemann, B. Korchin, T. Adams, C. Pico-Navarro, C. Heery, J. Schlom, J. L. Gulley, M. Bilusic, *J Immunother Cancer* **2021**, *9*, e003238.

[7] a) A. G. X. Zeng, S. Bansal, L. Jin, A. Mitchell, W. C. Chen, H. A. Abbas, M. Chan-Seng-Yue, V. Voisin, P. van Galen, A. Tierens, M. Cheok, C. Preudhomme, H. Dombret, N. Daver, P. A. Futreal, M. D. Minden, J. A. Kennedy, J. C. Y. Wang, J. E. Dick, *Nat. Med.* **2022**, *28*, 1212; b) A. E. Whiteley, T. T. Price, G. Cantelli, D. A. Sipkins, *Nat. Rev. Cancer* **2021**, *21*, 461; c) C. D. DiNardo, H. P. Erba, S. D. Freeman, A. H. Wei, *Lancet* **2023**, *401*, 2073; d) H. Kantarjian, T. Kadia, C. DiNardo, N. Daver, G. Borthakur, E. Jabbour, G. Garcia-Manero, M. Konopleva, F. Ravandi, *Blood Cancer J* **2021**, *11*, 41;

[8] a) X. Zhang, H. Cui, W. Zhang, Z. Li, J. Gao, *Bioact Mater* **2023**, *22*, 491; b) L. Ma, L. Diao, Z. Peng, Y. Jia, H. Xie, B. Li, J. Ma, M. Zhang, L. Cheng, D. Ding, X. Zhang, H. Chen, F. Mo, H. Jiang, G. Xu, F. Meng, Z. Zhong, M. Liu, *Adv. Mater.* **2021**, *33*, 2104849; c) S. A. Sadeghi Najafabadi, A. Bolhassani, M. R. Aghasadeghi, *Immunotherapy* **2022**, *14*, 639.

[9] a) J. Rosenblatt, R. M. Stone, L. Uhl, D. Neuberg, R. Joyce, J. D. Levine, J. Arnason, M. McMasters, K. Luptakova, S. Jain, J. I. Zwicker, A. Hamdan, V. Boussiotis, D. P. Steensma, D. J. DeAngelo, I. Galinsky, P. S. Dutt, E. Logan, M. P. Bryant, D. Stroopinsky, L. Werner, K. Palmer, M. Coll, A. Washington, L. Cole, D. Kufe, D. Avigan, *Sci. Transl. Med.* **2016**, *8*, 368ra171; b) V. T. Ho, H. T. Kim, N. Bavli, M. Mihm, O. Pozdnyakova, M. Piesche, H. Daley, C. Reynolds, N. C. Souders, C. Cutler, J. Koreth, E. P. Alyea, J. H. Antin, J. Ritz, G. Dranoff, R. J. Soiffer, *Blood Adv* **2017**, *1*, 2269.

[10] Y. Zheng, Z. Zhong, *J. Controlled Release* **2022**, *347*, 308.

[11] X. Cao, A. F. Cordova, L. Li, *Chem. Rev.* **2022**, *122*, 3414.

[12] a) S. Akira, S. Uematsu, O. Takeuchi, *Cell* **2006**, *124*, 783; b) Y. Hou, Y. Wang, Y. Tang, Z. Zhou, L. Tan, T. Gong, L. Zhang, X. Sun, *J. Controlled Release* **2020**, *326*, 120.

[13] a) S. Liu, Q. Jiang, X. Zhao, R. Zhao, Y. Wang, Y. Wang, J. Liu, Y. Shang, S. Zhao, T. Wu, Y. Zhang, G. Nie, B. Ding, *Nat. Mater.* **2021**, *20*, 421; b) N. F. Eng, N. Bhardwaj, R. Mulligan, F. Diaz-Mitoma, *Hum. Vaccines Immunother.* **2013**, *9*, 1661; c) Y. C. Zeng, O. J. Young, C. M. Wintersinger, F. M. Anastassacos, J. I. MacDonald, G. Isinelli, M. O. Dellacherie, M. Sobral, H. Bai, A. R. Graveline, A. Vernet, M. Sanchez, K. Mulligan, Y. Choi, T. C. Ferrante, D. B. Keskin, G. G. Fell, D. Neuberg, C. J. Wu, D. J. Mooney, I. C. Kwon, J. H. Ryu, W. M. Shih, *Nat. Nanotechnol.* **2024**.

[14] a) F. Ellouz, A. Adam, R. Ciorbaru, E. Lederer, *Biochem. Biophys. Res. Commun.* **1974**, *59*, 1317; b) R. Caruso, N. Warner, N. Inohara, G. Núñez, *Immunity* **2014**, *41*, 898.

[15] a) J. Overholser, K. H. Ambegaokar, S. M. Eze, E. Sanabria-Figueroa, R. Nahta, T. Bekaii-Saab, P. T. P. Kaumaya, *Vaccines* **2015**, *3*, 519; b) S. V. Guryanova, R. M. Khaitov, *Front Immunol* **2021**, *12*, 607178.

[16] E. M. Creagh, L. A. J. O'Neill, *Trends Immunol.* **2006**, *27*, 352.

[17] M. Aleynick, J. Svensson-Arvelund, C. R. Flowers, A. Marabelle, J. D. Brody, *Clin. Cancer Res.* **2019**, *25*, 6283.

[18] T. Shekarian, S. Valsesia-Wittmann, J. Brody, M. C. Michallet, S. Depil, C. Caux, A. Marabelle, *Ann. Oncol.* **2017**, *28*, 1756.

[19] a) G. A. Roth, V. C. T. M. Picece, B. S. Ou, W. Luo, B. Pulendran, E. A. Appel, *Nat. Rev. Mater.* **2022**, *7*, 174; b) J. M. Blander, R. Medzhitov, *Nature* **2006**, *440*, 808.

[20] N. K. Mehta, R. V. Pradhan, A. P. Soleimany, K. D. Moynihan, A. M. Rothschilds, N. Momin, K. Rakhra, J. Mata-Fink, S. N. Bhatia, K. D. Wittrup, D. J. Irvine, *Nat. Biomed. Eng.* **2020**, *4*, 636.

[21] a) D. T. Johnson, J. Zhou, A. V. Kroll, R. H. Fang, M. Yan, C. Xiao, X. Chen, J. Kline, L. Zhang, D.-E. Zhang, *Leukemia* **2022**, *36*, 994; b) X. Xie, Y. Hu, T. Ye, Y. Chen, L. Zhou, F. Li, X. Xi, S. Wang, Y. He, X. Gao, W. Wei, G. Ma, Y. Li, *Nat. Biomed. Eng.* **2021**, *5*, 414; c) N. J. Shah, A. J. Najibi, T.-Y. Shih, A. S. Mao, A. Sharda, D. T. Scadden, D. J. Mooney, *Nat. Biomed. Eng.* **2020**, *4*, 40; d) T. Ci, H. Li, G. Chen, Z. Wang, J. Wang, P. Abdou, Y. Tu, G. Dotti, Z. Gu, *Sci. Adv.* **2020**, *6*, eabc3013; e) Q. Hu, W. Sun, J. Wang, H. Ruan, X. Zhang, Y. Ye, S. Shen, C. Wang, W. Lu, K. Cheng, G. Dotti, J. F. Zeidner, J. Wang, Z. Gu, *Nat. Biomed. Eng.* **2018**, *2*, 831.

[22] a) J. Wei, D. Wu, S. Zhao, Y. Shao, Y. Xia, D. Ni, X. Qiu, J. Zhang, J. Chen, F. Meng, Z. Zhong, *Adv. Sci.* **2022**, *9*, 2103689; b) J. Wei, D. Wu, Y. Shao, B. Guo, J. Jiang, J. Chen, J. Zhang, F. Meng, Z. Zhong, *J. Controlled Release* **2022**, *347*, 68; c) G. Cui, Y. Sun, L. Qu, C. Shen, Y. Sun, F. Meng, Y. Zheng, Z. Zhong, *Adv. Healthcare Mater.* **2024**, *13*, 2303690.

[23] A. V. Krivtsov, D. Twomey, Z. Feng, M. C. Stubbs, Y. Wang, J. Faber, J. E. Levine, J. Wang, W. C. Hahn, D. G. Gilliland, T. R. Golub, S. A. Armstrong, *Nature* **2006**, *442*, 818.

[24] L. Yang, H. Fang, J. Jiang, Y. Sha, Z. Zhong, F. Meng, *Drug Deliv* **2022**, *12*, 2527.

[25] M. Liu, J. Zhang, X. Zhu, W. Shan, L. Li, J. Zhong, Z. Zhang, Y. Huang, *J. Controlled Release* **2016**, *222*, 67.

[26] A. J. van Beelen, Z. Zelinkova, E. W. Taanman-Kueter, F. J. Muller, D. W. Hommes, S. A. J. Zaat, M. L. Kapsenberg, E. C. de Jong, *Immunity* **2007**, *27*, 660.

[27] V. Pallarès, U. Unzueta, A. Falgàs, A. Aviñó, Y. Núñez, A. García-León, L. Sánchez-García, N. Serna, A. Gallardo, L. Alba-Castellón, P. Álamo, J. Sierra, L. Cedó, R. Eritja, A. Villaverde, E. Vázquez, I. Casanova, R. Mangues, *Biomaterials* **2022**, *280*, 121258.

[28] a) M. Norelli, B. Camisa, G. Barbiera, L. Falcone, A. Purevdorj, M. Genua, F. Sanvito, M. Ponzoni, C. Doglioni, P. Cristofori, C. Traversari, C. Bordignon, F. Ciceri, R. Ostuni, C. Bonini, M. Casucci, A. Bondanza, *Nat. Med.* **2018**, *24*, 739; b) N. Gong, X. Han, L. Xue, R. El-Mayta, A. E. Metzloff, M. M. Billingsley, A. G. Hamilton, M. J. Mitchell, *Nat. Mater.* **2023**, *22*, 1571.

[29] J. Yan, X. Liu, F. Wu, C. Ge, H. Ye, X. Chen, Y. Wei, R. Zhou, S. Duan, R. Zhu, Y. Zheng, L. Yin, *Adv. Mater.* **2022**, *34*, 2109517.

[30] L. Liu, X. Wan, P. Zhou, X. Zhou, W. Zhang, X. Hui, X. Yuan, X. Ding, R. Zhu, G. Meng, H. Xiao, F. Ma, H. Huang, X. Song, B. Zhou, S. Xiong, Y. Zhang, *J. Hematol. Oncol.* **2018**, *11*, 27.

[31] H. Sung, J. Ferlay, R. L. Siegel, M. Laversanne, I. Soerjomataram, A. Jemal, F. Bray, *Ca-Cancer J. Clin.* **2021**, *71*, 209.

[32] G. G. Zom, M. M. J. H. P. Willems, N. J. Meeuwenoord, N. R. M. Reintjens, E. Tondini, S. Khan, H. S. Overkleeft, G. A. van der Marel, J. D. C. Codee, F. Ossendorp, D. V. Filippov, *Bioconjugate Chem.* **2019**, *30*, 1150.

[33] a) K. T. Gause, Y. Yan, N. M. O'Brien-Simpson, J. Cui, J. C. Lenzo, E. C. Reynolds, F. Caruso, *Adv. Funct. Mater.* **2016**, *26*, 7526; b) N. A. Lind, V. E. Rael, K. Pestal, B. Liu, G. M. Barton, *Nat. Rev. Immunol.* **2022**, *22*, 224.

[34] a) E. Giannakopoulou, M. Lehander, S. Virding Culleton, W. Yang, Y. Li, T. Karpanen, T. Yoshizato, E. H. Rustad, M. M. Nielsen, R. C. Bollineni, T. T. Tran, M. Delic-Sarac, T. J. Gjerdingen, K. Douvlataniotis, M. Laos, M. Ali, A. Hillen, S. Mazzi, D. W. L. Chin, A. Mehta, J. S. Holm, A. K. Bentzen, M. Bill, M. Griffioen, T. Gedde-Dahl, S. Lehmann, S. E. W. Jacobsen, P. S. Woll, J. Olweus, *Nat Cancer* **2023**, *4*, 1474; b) F. P. Tambaro, H. Singh, E. Jones, M. Rytting, K. M. Mahadeo, P. Thompson, N. Daver, C. DiNardo, T. Kadia, G. Garcia-Manero, T. Chan, R. R. Shah, W. G. Wierda, *Leukemia* **2021**, *35*, 3282; c) K. Knorr, J. Rahman, C. Erickson, E. Wang, M. Monetti, Z. Li, J. Ortiz-Pacheco, A. Jones, S. X. Lu, R. F. Stanley, M. Baez, N. Fox, C. Castro, A. E. Marino, C. Jiang, A. Penson, S. J. Hogg, X. Mi, H. Nakajima, H. Kunimoto, K. Nishimura, D. Inoue, B. Greenbaum, D. Knorr, J. Ravetch, O. Abdel-Wahab, *Nat Cancer* **2023**, *4*, 1675.

[35] C. S. K. Leung, B. J. Van den Eynde, *Cancer Cell* **2022**, *40*, 903.